Probing statistics of coherent states by continuous wave mixing on a single artificial atom

A. Yu. Dmitriev,[1,*] R. Shaikhaidarov,[2] T. Hönigl-Decrinis,[2,3]
S. E. de Graaf,[3] V. N. Antonov,[2,4,1] and O. V. Astafiev[2,3,1,†]

[1] *Moscow Institute of Physics and Technology, 141700 Dolgoprudny, Russia*
[2] *Physics Department, Royal Holloway, University of London, Egham, Surrey TW20 0EX, United Kingdom*
[3] *National Physical Laboratory, Teddington, TW11 0LW, United Kingdom*
[4] *Skolkovo Institute of Science and Technology, Nobel str. 3, 143026 Moscow, Russia*

(Dated: May 7, 2019)

We study four- and higher-order wave mixing of continuous coherent waves on a single superconducting artificial atom. Narrow side peaks of different orders of nonlinearity resulting from elastic multi-photon scattering on the atom are observed and investigated. We derive an analytical expression for the peak amplitudes and show that the ratio of any two adjacent peaks is a function of driving amplitudes and detuning. This is attributed to the photon distribution in the coherent states and provides a measure for characterisation of photon statistics in non-classical coherent waves. We also demonstrate an Autler-Townes-like splitting of side peaks, the magnitude of which scales with the scattering order.

The superconducting quantum circuits [1, 2] strongly coupled to either confined [3] or propagating [4] electromagnetic waves become an especially advantageous toolkit for the demonstration of quantum optical phenomena in the microwave frequency domain [5], offering conditions which are not achievable with natural atoms. Some striking examples are the demonstration of strong [6–8] and ultra-strong [9–11] coupling of light to a single qubit, the coupling of qubits by virtual photons [12], the dynamical Casimir effect [13], sources of single photons [14, 15] and entangled propagating photons [16], lasing [17] and amplification [8] with a single artificial atom. A range of specific effects related to the intrinsic nonlinearity of an atom were demonstrated, for example, the phase shift acquired by single propagating photons [18], or the preparation of cat states in the cavity [19]. In general, the nonlinearity is a tool for the implementations of quantum gates, as described in various proposals [20–23]. Therefore, the nonlinear regimes of light-matter interactions in circuit-QED are of specific importance and interest for both fundamental quantum optics and quantum information processing.

Wave mixing in optical media is one of the basic nonlinear parametric processes. In particular, four-wave mixing occurs due to the third-order susceptibility $\chi^{(3)}$ of a media, which gives the polarization term $P^{(3)} = \chi^{(3)}E^3$, proportional to third power of electric field E. If three electromagnetic waves with frequencies ω_1, ω_2, ω_3 propagate through the media, a number of additional waves appears with frequencies $\pm\omega_i \pm \omega_j \pm \omega_k$, where $i, j, k = \{1, 2, 3\}$ [24], and their amplitudes and phases are controlled by the initial waves. The corresponding scattering process requires absorption/emission of three photons from source waves, and generates one extra photon. With higher $2p + 1$ odd-order nonlinearity, where p is a non-negative integer number, the processes is characterised by $\chi^{(2p+1)}$ and one extra photon is generated as a result of interaction between $2p + 1$ photons. A wide range of applications of wave mixing in various systems includes generation of squeezed states of light [25–27], parametric amplification [28], frequency conversion and generation of frequency combs [29]. For superconducting quantum circuits, the effect of wave mixing [30] of short microwave pulses was observed and characterised. Very recently, it was shown that a strongly driven two-level system could amplify a weak probe in between the components of the Mollow triplet due to four-photon processes [31]. Three-wave mixing was also theoretically described for cyclic artificial atoms [32], and experimentally observed [33] on a single three-level circuit.

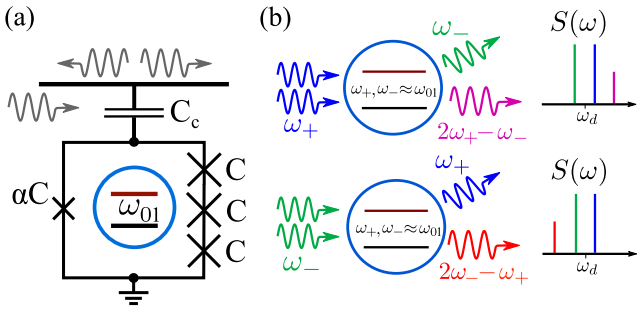

FIG. 1. **(a)** Schematics of the device. The artificial atom is a 4-junction flux qubit with three nearly identical junctions with capacitance C and one junction with capacitance αC, where $\alpha = 0.43$. The qubit is coupled to a coplanar waveguide with capacitance C_c. **(b)** The wave mixing of two tones on a single two-level system. With the two-photon absorption and one photon emission at frequencies $\omega_\pm$ and $\omega_\mp$ one more photon is generated at frequency $2\omega_\pm - \omega_\mp$ resulting in corresponding side frequency emissions.

In our work, we study the wave mixing of continuous coherent waves on a single superconducting qubit as a two-level artificial atom strongly coupled to a coplanar

waveguide. An atom is irradiated by two propagating microwaves at frequencies close to resonance. We measure narrow sideband spectral peaks [34] attributed to elastic multi-photon scattering processes of four-, six- and higher-orders. With two waves incoming to the qubit, the scattering process of any order is allowed due to (i) high-order nonlinear terms provided by the qubit; (ii) the finite probability of finding any photon number in the classical states (which are coherent states with Poissonian photon statistics). The side peak intensities depend on the order of nonlinear processes, incident wave amplitudes, and their detuning from the atomic transition. An interesting feature is that with the coherent wave scattering the ratio between consequent peak intensities is independent on the peak orders, which is confirmed both experimentally and theoretically. With a strong drive, the side peak intensities exhibit splitting in frequency domain with the magnitude proportional to the driving amplitudes. This is similar to the Autler-Townes splitting, (studied also in superconducting circuits [6, 35–37]), however, the corresponding splitting magnitude is inversely proportional to the order of the scattering process. We derive an analytical expression for the spectra and obtain a good agreement with the experimental data.

We begin with considering a two-level atom with transition frequency ω_{01}, see Fig. 1(a). The atom is strongly coupled to a transmission line (open space) with the radiative relaxation rate Γ_1 due to the photon emission into the line. The strong coupling condition implies that non-radiative relaxation (without emission of the photon to the line) Γ_1^{nr} and pure dephasing rates γ are smaller than Γ_1. A driving monochromatic wave with frequency ω_d and wavevector k described by voltage amplitude $V_0 e^{-i\omega_d t+ikx}$ propagates through the waveguide and scatters on the atom located at $x=0$. As a result, the wave is scattered elastically and inelastically either forward or backward. The amplitude of the elastically scattered wave $V^{sc}e^{-i\omega_d t+ik|x|}$ is expressed as

$$V^{sc} = -\frac{i\Gamma_1}{\hbar\mu}\langle\sigma^-\rangle, \tag{1}$$

where σ^- is the atomic state annihilation operator and μ is the atomic dipole moment. Here we will not consider an inelastically scattered radiation. By finding the stationary solution of the master equation for the atom with the external drive, it can be shown [4] that the amplitude of the elastically scattered wave $V^{sc}e^{-i\omega_d t+ik|x|}$ is expressed as

$$V^{sc} = -rV_0 = -\frac{V_0}{2}\frac{\lambda\Gamma_1}{|\lambda|^2+\Omega^2\Gamma_2/\Gamma_1}, \tag{2}$$

where $\lambda = \Gamma_2 + i\Delta\omega$, $\Delta\omega = \omega_d - \omega_{01}$ is detuning, $\Gamma_2 = \frac{\Gamma_1+\Gamma_1^{nr}}{2}+\gamma$ is the full dephasing rate, $\Omega = \mu V_0/\hbar$ is the driving amplitude of the incident wave, and r is reflection coefficient. One important consequence of Eq. (2) is that in a weak driving limit ($\Omega \ll \Gamma_1$) with $\Gamma_2 = \Gamma_1/2$ (ideal strong coupling: $\Gamma_1^{nr} = \gamma = 0$) and $\lambda = \Gamma_1/2$ at $\Delta\omega = 0$, the scattered wave is equal to the incident wave in amplitude but negative in sign: $V^{sc} = -V_0$.

Next, we generalise the problem to the scattering of two coherent waves at frequencies $\omega_+ = \omega_d + \delta\omega$ and $\omega_- = \omega_d - \delta\omega$, as depicted in Fig. 1(b), where the frequency shift is small: $\delta\omega \ll \Gamma_1$. The mixing processes can be described in terms of multi-photon elastic scattering. In particular, Fig. 1(b) illustrates four-wave mixing processes ($2p+1=3$). The upper panel describes a mechanism of a photon generation at $2\omega_+ - \omega_-$ as a result of the four-photon process: two photons from the ω_+–mode are absorbed and two photons are emitted, one at ω_- and one at $2\omega_+ - \omega_-$. The lower panel represents a symmetric process with emission of a photon at $2\omega_- - \omega_+$. These two processes are called degenerate four-wave mixing and can be spectroscopically detected by observation of side spectral peaks at corresponding frequencies. As a probability to find an arbitrary number of photons in coherent states is finite, any higher-order processes take place. They result in creation of the spectral components at $\omega_{\pm(2p+1)} = (p+1)\omega_\pm - p\omega_\mp$ as an outcome of scattering with $2p+1$ photons involved, where $p \geq 0$ is an integer. We are measuring the continuous mixing of two coherent waves on a superconducting quantum system strongly coupled to a transmission line.

The artificial atom in our device is a flux qubit coupled to a coplanar waveguide by capacitance $C_c = 2$ fF (Fig. 1(a)), which also effectively shunts the α-junction [30]. The persistent current is estimated to be quite small, $I_p = 52$ nA, however, the anharmonicity $\omega_{12} - \omega_{01} \approx 2\pi \times 1.5$ GHz is still large to not account for higher levels. Other important parameters are the energy splitting at the degeneracy point $\Delta_q = 2\pi \times 7.30$ GHz and rates of relaxation and decoherence $\Gamma_1/2\pi = 2.2$ MHz and $\Gamma_2/2\pi = 1.1$ MHz measured at $\omega_{01} = \Delta_q$. To measure the transmission coefficient of a waveguide with the embedded qubit, we built a standard low-temperature setup described elsewhere [8]. The qubit is located at the 15 mK-flange in a dilution refrigerator. The input microwave signals with very narrow spectral widths of ~ 1 Hz are delivered to the chip via coaxial lines with attenuators at different temperature stages used to suppress the room-temperature blackbody radiation. The output signals go through a microwave isolator and are amplified by a cryogenic HEMT amplifier situated at 4K stage of the refrigerator and then by two microwave amplifiers at room temperature.

The transmitted waves can be measured by a vector network analyzer or by a spectrum analyzer. Preliminary calibration is performed by measuring the transmission coefficient $t = V_{tr}/V_0$ of a single microwave tone of frequency $\omega_d \approx \omega_{01}$, and using the relation $r + t = 1$. We calculate the value of the reflection coefficient r and fit it using Eq. (2). The result is shown in Fig. 2(a). By fit-

ting the peak, we obtain a value of Ω for a certain output level of the microwave generator and thereby we can determine the amplitude of the driving signal, see Fig. 2(a).

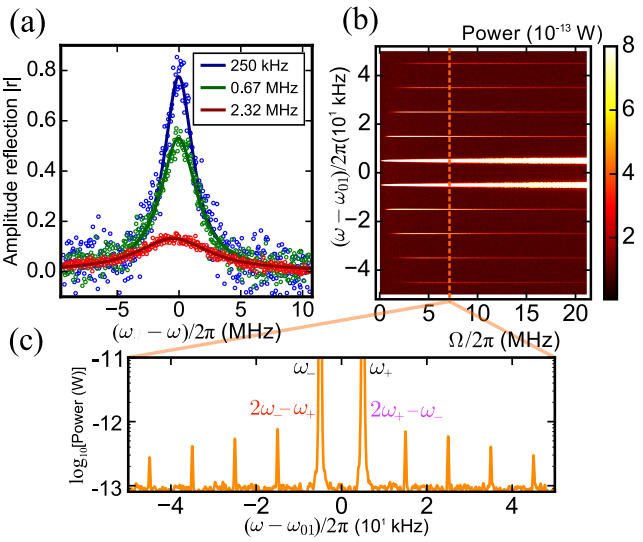

FIG. 2. **(a)** The single frequency wave elastically scattered from the artificial atom: blue dots correspond to a weak drive. At higher powers, the atom is saturated and the reflection is reduced (green and red dots). Solid lines are fits made using Eq. (2). The legend captions are values of $\Omega/2\pi$ extracted from the fit. **(b)** The spectra of coherently scattered radiation measured by a spectrum analyser when driving tones are resonant with the qubit, plotted as a function of the amplitude of both tones: $\Omega_+ = \Omega_- = \Omega$. **(c)** An example of a typical spectrum.

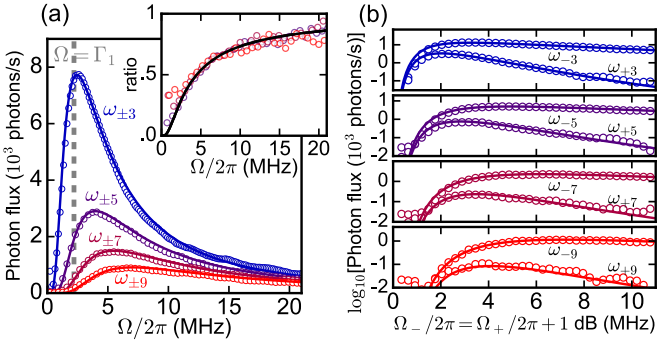

FIG. 3. **(a)** Sideband spectral components of elastically scattered waves. Experimental points obtained with $\delta\omega/2\pi = 5$ kHz, are fitted with Eq. (7) (solid lines) with parameters $\Gamma_1/2\pi = 2.2$ MHz, $\Gamma_2/2\pi = 1.1$ MHz, $\Delta\omega/2\pi = 0$, $\Omega_+ = \Omega_- = \Omega$ and $p = 1, 2, 3, 4$ for each curve, respectively. Inset shows the ratio of photon fluxes in components of consequent order $2p+1$ and $2p+3$ for $p = 1, 2, 3$. The black line represents the direct evaluation of ratios from Eq.(8). **(b)** The wave mixing for asymmetric driving signals: Ω_- is larger by 1 dB than Ω_+. The photon flux in negative side components is a few times larger than the positive ones. This demonstrates the high sensitivity of wave mixing to the imbalance of the driving amplitudes.

For the demonstration of wave mixing, we tune the qubit to the degeneracy point $\omega_{01} = \Delta_q$ and apply two microwaves at frequencies $\omega_+ = \omega_d + \delta\omega$ and $\omega_- = \omega_d - \delta\omega$, as depicted in Fig. 2(b). The detuning $\delta\omega/2\pi$ is typically chosen to be 1 - 100 kHz $\ll \Gamma_1/2\pi, \Gamma_2/2\pi$, therefore both tones are within the width of the resonance line ($\sim \Gamma_2$) with a qubit but still easily distinguishable. By measuring the spectrum of the output signal, we observe many side spectral components at frequencies $\omega_{\pm(2p+1)} = \omega_d \pm (2p+1)\delta\omega$, where $p > 0$ is an integer, see Fig. 2(b, c). Figure 3(a) demonstrates the side peak amplitudes for $1 < p < 4$ (up to 9-photon process) with $\Omega_+ = \Omega_- = \Omega$ as a function of the driving amplitude Ω: left and right hand-side peaks are of equal amplitudes. With the increase of Ω, the side peak amplitudes reach maxima and then decay. With increasing the order of the processes the maxima are obtained for a higher driving amplitude. We interpret this in the following way. The peak order $(2p+1)$ corresponds to the number of interacting photons. The photon absorption/emission rate is determined by the Rabi-oscillation frequency, equivalent to the driving amplitude Ω. The characteristic interaction time determined by the system coherence is $\tau \approx \Gamma_2^{-1}$. Therefore, to efficiently absorb/emit $2p+1$ photons, one needs to drive the system with the amplitude $2\Omega\tau \approx 2p+1$ (here we take $\Omega_- + \Omega_+ = 2\Omega$) and we obtain $\Omega_{max} \approx \Gamma_1(2p+1)/4$ (we take $\Gamma_2 = \Gamma_1/2$).

We also investigate how the intensities of the side peaks depend on the difference in amplitudes of the driving waves, when $\Omega_- \neq \Omega_+$. To illustrate that we vary both driving amplitudes while keeping the amplitude Ω_- 1 dB (1.26 times in amplitude) higher than Ω_+ and measure the side-band components (Fig. 3(b)). The symmetry is now broken and the intensities at $\omega_{-(2k+1)}$ become several times larger than at $\omega_{+(2k+1)}$. The processes generating positive frequency peaks become less probable than the ones resulting in negative frequency components. This is a direct consequence of having more photons in the ω_-–mode.

Next, we study an effect of detuning $\Delta\omega = \omega_d - \omega_{01}$ by varying the central frequency ω_d with fixed $\delta\omega$. We measure the spectral components of the signal at frequencies $\omega_{\pm(2p+1)}$ as a function fof $\Omega_\pm$ in the condition of $\Omega_- = \Omega_+ = \Omega$. The observed effect is similar to Autler-Townes splitting, see Fig. 4 [36]. The mixed signals of each order are split into two peaks with maxima at $\Delta\omega_{max} \approx \pm\zeta_p\Omega$, where ζ_p is a constant inversely proportional to $2p+1$. The peak position at a strong drive ($\Delta\omega \gg \Gamma_2$) can be estimated in a similar way as we have done it above for the peak maximum. To estimate $\Delta\omega_{max}$ we substitute the characteristic time Γ_2^{-1} by $\tau \approx \Delta\omega^{-1}$. The peak maximum is then expected for $\zeta_p = \Delta\omega_{max}/\Omega \approx 4/(2p+1)$.

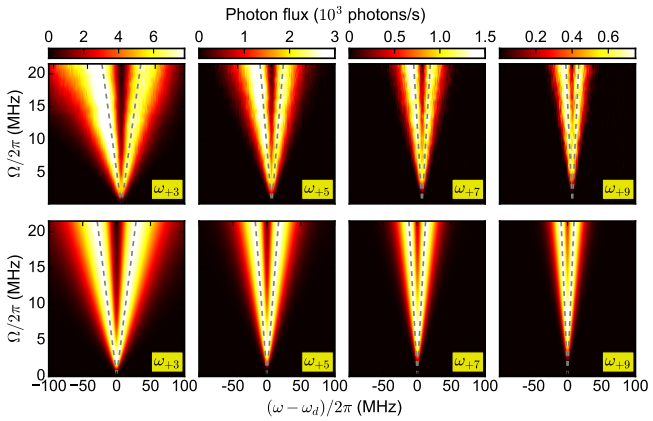

FIG. 4. The Autler-Townes-like splitting of side spectral components of scattered radiation as a function of the central frequency detuning and driving amplitudes Ω. The upper panels represent measured splittings. Lower panels represent analytical calculations with Eq. (8). Grey dashed lines are the guidelines corresponding to $\Delta\omega = 4\Omega/(2p+1)$.

To quantitatively analyze the amplitudes of the wave mixing side peaks we consider the Hamiltonian of a single two-level system driven by two classical (coherent) waves

$$H = -\frac{\hbar\omega_{01}}{2}\sigma_z - \hbar\Omega_-\sigma_x\cos(\omega_d t - \delta\omega t) - \hbar\Omega_+\sigma_x\cos(\omega_d t + \delta\omega t), \quad (3)$$

where Ω_+ and Ω_- are amplitudes of the drives. First, we calculate a stationary solution for the master equation in the Rotating Wave Approximation. The term $\delta\omega t$ is interpreted here as a slowly varying phase because $\delta\omega t \ll 1$ on a time scale $t \sim \Gamma_2^{-1}$. An analytical solution for the expectation value of the atomic annihilation operator is

$$\langle\sigma^-\rangle = -\frac{\sin\theta}{\Lambda}\frac{\Omega_- e^{-i\delta\omega t} + \Omega_+ e^{i\delta\omega t}}{1+\sin\theta\cos 2\delta\omega t}. \quad (4)$$

Here we introduce the following notations: $\theta = \arcsin\left(\frac{2\Gamma_2\Omega_-\Omega_+}{\Gamma_1|\lambda|^2+\Gamma_2(\Omega_-^2+\Omega_+^2)}\right)$, $\Lambda^{-1} = \frac{\lambda\Gamma_1}{4\Gamma_2\Omega_-\Omega_+}$. The denominator of Eq. (4) can be rearranged according to

$$\frac{1}{1+\frac{1}{2}\sin\theta(z+z^{-1})} = \frac{1}{\cos\theta}\left(\frac{1}{1-yz}+\frac{1}{1-yz^{-1}}-1\right), \quad (5)$$

where $z = e^{2i\delta\omega t}$ and $y = -\tan\frac{\theta}{2}$. We expand the right part of Eq. (5) into power series in z and arrive at

$$\langle\sigma^-\rangle = -\frac{\Omega_- e^{-i\delta\omega t} + \Omega_+ e^{i\delta\omega t}}{\Lambda}\tan\theta\sum_{p=-\infty}^{\infty} y^{|p|}e^{i2p\delta\omega t}. \quad (6)$$

Taking into account Eq. (1) and transforming the sum to non-negative p, we obtain

$$V^{sc} = -\frac{\hbar\Gamma_1\tan\theta}{\mu\Lambda}\sum_{p=0}^{\infty} y^p\Big[(\Omega_- + y\Omega_+)e^{-i(2p+1)\delta\omega t} + (y\Omega_- + \Omega_+)e^{i(2p+1)\delta\omega t}\Big]. \quad (7)$$

With the relations between the driving amplitude and the voltage amplitude $V_\pm\mu = \hbar\Omega_\pm$, we arrive to the analytical expression for the amplitude of each side spectral component

$$V^{sc}_{\pm(2p+1)} = \frac{(-1)^p\Gamma_1\tan\theta\tan^p\frac{\theta}{2}}{\Lambda}(V_\mp\tan\frac{\theta}{2} - V_\pm), \quad (8)$$

which can be verified experimentally. Eq. (8) shows that the factor $\tan^p\frac{\theta}{2}$ contains all the dependence of spectral components on the order p. To exemplify that, we also deduce ratios of consequent components of order $2p+1$ and $2p+3$ for the data presented in Fig. 3 and present the result in the inset of Fig. 3(a) for $p = 1, 2, 3$. Notice that it is the same for each pair independently of p, and fits well with the black solid line derived from Eq.(8). The result is valid for classical coherent states, in which photon statistics is given by the Poissonian distribution.

We now compare the experimental data with our analytical expression of Eq. (8). Solid lines in Fig. 3 show the calculated peak dependences, which are in good agreement with the experimental data. Analysing Eq. (8) for extrema, we find that the peak maxima are well explained by the asymptotic relation $\Omega_{max} \approx \sqrt{2}\Gamma_1(2p+1)/4$, which is consistent with our preliminary qualitative prediction and the physical picture we provide. Also, the driving amplitude dependence versus detuning reproduces well the measurement as it is shown in Fig. 4. Quantitative analysis of Eq. (8) gives maximal response at $\omega_{max}/\Omega \approx 4/(2p+1)$.

Next, we illustrate that the wave mixing spectral components reveal photon statistics of the incident waves. In the strong coupling and weak driving regime ($\Omega_\pm \ll \Gamma_1$), the scattered photon number into the mode ω_{2p+1} in one direction is simplified from Eq. (8) to

$$\langle N_{2p+1}\rangle \approx \langle N_-\rangle^p\langle N_+\rangle^{p+1}, \quad (9)$$

where $\langle N_k\rangle = \Omega_k^2/\Gamma_1\Gamma_2$ is the mean photon number in the mode ω_k on the characteristic time interval $\tau = \Gamma_2^{-1}$. Remarkably, this is equivalent to the expectation value of the operator $(a_+a_-^\dagger)^p a_+$ averaged over the states $|\alpha_-\alpha_+\rangle$. Its squared value is $|\langle(a_+a_-^\dagger)^p a_+\rangle|^2 \approx |(\alpha_-^*)^p\alpha_+^{p+1}|^2 = \langle N_-\rangle^p\langle N_+\rangle^{p+1}$. The prefactors $(\alpha_-^*)^p$ and α_+^{p+1} are determined by probability amplitudes of the corresponding photon states ($|p\rangle_-$ and $|p+1\rangle_+$). For instance, in the weak driving regime $\alpha \ll 1$ and $\langle a^n\rangle \approx \langle\alpha|\, a^n\frac{\alpha^n}{\sqrt{n!}}\,|n\rangle = \langle 0|\alpha^n|0\rangle = \alpha^n$, that is approximately equal to the probability amplitude of the photon-number state $|n\rangle$ in the

coherent state $|\alpha\rangle$ multiplied by $\sqrt{n!}$. The case with deviation from the classical coherent states has been already discussed though in a different regime of pulsed dynamics [30]. We believe that our method is promising for detection and characterisation of non-classical coherent states. An example of practical application is the setup where the calibrated classical signal is applied to the qubit in the ω_+-mode, and in ω_--mode the quantum signal is applied where the photon statistics deviates from the Poissonian one. In this case, the intensities of elastic sidebands, like the ones we presented at Fig. 3, could be used for full reconstruction of the photon statistics of the quantum state.

In conclusion, we have demonstrated a fundamental effect of wave mixing of stationary coherent states on a single two-level scatterer strongly coupled to a one-dimensional transmission line. We derive an analytical expression for the amplitudes of mixed states and have shown a series of other physical effects, for example, an Autler-Townes-like splitting of side peaks dependent on the number of scattered photons. The side peaks are results of multi-photon scattering processes and their amplitudes determined by the photon distribution in the coherent states. An interesting future application would be to visualize statistics of nonclassical coherent states.

This research is supported by the Russan Science Foundation, grant No. 16-12-00070, and by Russian Foundation of Basic Research, grant 19-32-80006. We are grateful to A. Semenov for useful discussions.

* dmitrmipt@gmail.com
† Oleg.Astafiev@rhul.ac.uk

[1] J. Clarke and F. K. Wilhelm, Nature **453**, 1031 (2008).
[2] M. H. Devoret and R. J. Schoelkopf, Science **339**, 1169 (2013).
[3] A. Wallraff, D. I. Schuster, A. Blais, L. Frunzio, R.-S. Huang, J. Majer, S. Kumar, S. M. Girvin, and R. J. Schoelkopf, Nature **431**, 162 (2004).
[4] O. Astafiev, A. M. Zagoskin, A. Abdumalikov, Y. A. Pashkin, T. Yamamoto, K. Inomata, Y. Nakamura, and J. Tsai, Science **327**, 840 (2010).
[5] X. Gu, A. F. Kockum, A. Miranowicz, Y. xi Liu, and F. Nori, Physics Reports **718-719**, 1 (2017).
[6] A. A. Abdumalikov, O. Astafiev, A. M. Zagoskin, Y. A. Pashkin, Y. Nakamura, and J. S. Tsai, Phys. Rev. Lett. **104**, 193601 (2010).
[7] I.-C. Hoi, C. Wilson, G. Johansson, J. Lindkvist, B. Peropadre, T. Palomaki, and P. Delsing, New Journal of Physics **15**, 025011 (2013).
[8] O. V. Astafiev, A. A. Abdumalikov, A. M. Zagoskin, Y. A. Pashkin, Y. Nakamura, and J. S. Tsai, Phys. Rev. Lett. **104**, 183603 (2010).
[9] T. Niemczyk, F. Deppe, H. Huebl, E. Menzel, F. Hocke, M. Schwarz, J. Garcia-Ripoll, D. Zueco, T. Hümmer, E. Solano, *et al.*, Nature Physics **6**, 772 (2010).
[10] P. Forn-Díaz, J. Lisenfeld, D. Marcos, J. J. García-Ripoll, E. Solano, C. J. P. M. Harmans, and J. E. Mooij, Phys. Rev. Lett. **105**, 237001 (2010).
[11] P. Forn-Díaz, J. García-Ripoll, B. Peropadre, J.-L. Orgiazzi, M. Yurtalan, R. Belyansky, C. Wilson, and A. Lupascu, Nature Physics **13**, 39 (2017).
[12] A. F. van Loo, A. Fedorov, K. Lalumière, B. C. Sanders, A. Blais, and A. Wallraff, Science **342**, 1494 (2013).
[13] C. M. Wilson, G. Johansson, A. Pourkabirian, M. Simoen, J. R. Johansson, T. Duty, F. Nori, and P. Delsing, Nature **479**, 376 (2011).
[14] Z. Peng, S. De Graaf, J. Tsai, and O. Astafiev, Nature Communications **7**, 12588 (2016).
[15] P. Forn-Díaz, C. W. Warren, C. W. S. Chang, A. M. Vadiraj, and C. M. Wilson, Phys. Rev. Applied **8**, 054015 (2017).
[16] S. Gasparinetti, M. Pechal, J.-C. Besse, M. Mondal, C. Eichler, and A. Wallraff, Phys. Rev. Lett. **119**, 140504 (2017).
[17] O. Astafiev, K. Inomata, A. Niskanen, T. Yamamoto, Y. A. Pashkin, Y. Nakamura, and J. Tsai, Nature **449**, 588 (2007).
[18] I.-C. Hoi, A. F. Kockum, T. Palomaki, T. M. Stace, B. Fan, L. Tornberg, S. R. Sathyamoorthy, G. Johansson, P. Delsing, and C. M. Wilson, Phys. Rev. Lett. **111**, 053601 (2013).
[19] G. Kirchmair, B. Vlastakis, Z. Leghtas, S. E. Nigg, H. Paik, E. Ginossar, M. Mirrahimi, L. Frunzio, S. M. Girvin, and R. J. Schoelkopf, Nature **495**, 205 (2013).
[20] G. J. Milburn, Phys. Rev. Lett. **62**, 2124 (1989).
[21] D. J. Brod and J. Combes, Phys. Rev. Lett. **117**, 080502 (2016).
[22] W. J. Munro, K. Nemoto, and T. P. Spiller, New Journal of Physics **7**, 137 (2005).
[23] Q. Lin and J. Li, Phys. Rev. A **79**, 022301 (2009).
[24] R. W. Boyd, *Nonlinear optics* (Academic press, 2003).
[25] R. Slusher, L. Hollberg, B. Yurke, J. Mertz, and J. Valley, Physical Review Letters **55**, 2409 (1985).
[26] C. Eichler, D. Bozyigit, C. Lang, M. Baur, L. Steffen, J. M. Fink, S. Filipp, and A. Wallraff, Phys. Rev. Lett. **107**, 113601 (2011).
[27] D. M. Toyli, A. W. Eddins, S. Boutin, S. Puri, D. Hover, V. Bolkhovsky, W. D. Oliver, A. Blais, and I. Siddiqi, Phys. Rev. X **6**, 031004 (2016).
[28] M. Castellanos-Beltran, K. Irwin, G. Hilton, L. Vale, and K. Lehnert, Nature Physics **4**, 929 (2008).
[29] T. J. Kippenberg, R. Holzwarth, and S. Diddams, Science **332**, 555 (2011).
[30] A. Y. Dmitriev, R. Shaikhaidarov, V. Antonov, T. Hönigl-Decrinis, and O. Astafiev, Nature Communications **8**, 1352 (2017).
[31] P. Wen, A. Kockum, H. Ian, J. Chen, F. Nori, and I.-C. Hoi, Phys. Rev. Lett. **120**, 063603 (2018).
[32] Y.-x. Liu, H.-C. Sun, Z. Peng, A. Miranowicz, J. Tsai, and F. Nori, Scientific Reports **4**, 7289 (2014).
[33] T. Hönigl-Decrinis, I. V. Antonov, R. Shaikhaidarov, V. Antonov, A. Y. Dmitriev, and O. Astafiev, Phys. Rev. A **98**, 041801(R) (2018).
[34] B. R. Mollow, Phys. Rev. **188**, 1969 (1969).
[35] M. Baur, S. Filipp, R. Bianchetti, J. M. Fink, M. Göppl, L. Steffen, P. J. Leek, A. Blais, and A. Wallraff, Phys. Rev. Lett. **102**, 243602 (2009).
[36] M. A. Sillanpää, J. Li, K. Cicak, F. Altomare, J. I. Park, R. W. Simmonds, G. S. Paraoanu, and P. J. Hakonen, Phys. Rev. Lett. **103**, 193601 (2009).

[37] Z. H. Peng, J. H. Ding, Y. Zhou, L. L. Ying, Z. Wang, L. Zhou, L. M. Kuang, Y.-x. Liu, O. V. Astafiev, and J. S. Tsai, Phys. Rev. A **97**, 063809 (2018).